Supporting information for

Core-shell Fe_3O_4@$CoFe_2O_4$ nanoparticles as high-performance anode catalysts for enhanced oxygen evolution reaction

Lisa Royer,[a,b] Iryna Makarchuk,[b] Simon Hettler,[c,d] Raul Arenal, [c,d,e] Tristan Asset,[a] Benjamin Rotonnelli,[a] Antoine Bonnefont,[f] Elena Savinova,[a] Benoit P. Pichon*[,b,g]

[a] ICPEES, UMR 7515 CNRS-ECPM-Université de Strasbourg, 25, rue Becquerel, F 67087 Strasbourg cedex 2, France
[b] Université de Strasbourg, CNRS, Institut de Physique et Chimie des Matériaux de Strasbourg, UMR 7504, F-67000 Strasbourg, France
[c] Instituto de Nanociencia y Materiales de Aragon (INMA), CSIC-Universidad de Zaragoza, Calle Pedro Cerbuna 12, 50009 Zaragoza, Spain
[d] Laboratorio de Microscopías Avanzadas (LMA), Universidad de Zaragoza, Calle Mariano Esquillor, 50018 Zaragoza, Spain
[e] ARAID Foundation, 50018 Zaragoza, Spain
[f] Institut de Chimie, UMR 7177, CNRS-Université de Strasbourg, 4 rue Blaise Pascal, CS 90032, 67081 Strasbourg cedex, France
[g] Institut Universitaire de France, 5 rue Descartes, 75 015 Paris

Table of Contents

Experimental Procedures

1) Nanoparticle synthesis

Iron oxide core-shell NPs:

Four different types of core-shell NPs were synthesized aiming for different sizes of the core and of the shell.

- CS-1:

The iron oxide NPs were synthesized an already published protocol[1]. A two-necked round-bottom flask was filled with 1.38 g (2.22 mmol) of iron (II) stearate, 1.254 g (4.44 mmol) of oleic acid (99% Alfa Aesar) and 20 mL of ether dioctyl (BP = 290 °C, 97% Fluka). The brownish mixture was heated at 100 °C under a magnetic stir for 30 min in order to remove water residues and to homogenize the solution. The magnetic stirrer was then removed and the flask was connected to a reflux condenser before heating the solution to reflux for 2 h with a heating ramp of 5 °C/min. At the end, the mixture was allowed to cool to 100 °C. 4 mL of the solution was kept to analyze following an already published protocol[2]. After cooling these 4mL at room temperature, the NPs were precipitated by the addition of acetone and washed by agitation with a magnetic stirrer in warm acetone (60°).
After a cooling down the rest of the solution, 0.29 g (0.46 mmol) of cobalt (II) stearate, 0.791 g (2.8 mmol) of oleic acid, and 32 mL of 1-octadecene were added to the reaction medium. The mixture was heated to 100 °C for 30 min under magnetic stirring to remove water residues and to homogenize the solution. After removal of the magnetic stirrer, 0.585 g (0.94 mmol) of iron (II) stearate was added. The flask was then connected to a reflux condenser to heat the solution at reflux for another 2 h with a heating ramp of 1 °C/min. After cooling to room temperature, the nanoparticles were precipitated by the addition of acetone and then washed by centrifugation in a mix of chloroform and acetone. They were then stored in chloroform.

- CS-2:

The iron oxide NPs were synthesized an already published protocol[1].A two-necked round-bottom flask was filled with 1.38 g (2.22 mmol) of iron (II) stearate, 1.254 g (4.44 mmol) of oleic acid (99% Alfa Aesar) and 20 mL of ether dioctyl (Bp = 290 °C, 97% Fluka). The brownish mixture was heated at 100 °C under a magnetic stir for 30 min in order to remove water residues and to homogenize the solution. The magnetic stirrer was then removed and the flask was connected to a reflux condenser before heating the solution to reflux for 2 h with a heating ramp of 5 °C/min. At the end, the mixture was allowed to cool to 100 °C. 4 mL of the solution was kept to analyze: after cooling these 4mL at room temperature, the NPs were precipitated by the addition of acetone and washed by agitation with a magnetic stirrer in warm acetone (60°). Then, the shell was synthesized adapting an already published protocol[3].
After a cooling down step 0.335 g (0.531mmol) of cobalt stearate (II) was dissolved in 20 mL of octadecene and subsequently added to the remaining solution. The reaction medium was heated again at 100°C for 30 minutes under magnetic stirring to remove water residues and to homogenize the solution. After removal of the magnetic stirrer, the flask was connected to a reflux condense to heat the solution at reflux for 3 h under air with a heating rate of 1°C/min. Finally, after cooling to room temperature, the nanoparticles were precipitated by the addition of acetone to wash them by agitation with a magnetic stirrer in warm acetone (60°) for 1 hour. They were then stored in chloroform

- CS-3:

The iron oxide core of the NPs was synthesized using iron stearate (III), the synthesis protocol was developed by F. Perton[4]. A two-necked round-bottom flask was filled with 2 g (2.2 mmol) of commercial iron (III) stearate, 1.23 g of oleic acid (99% Alfa Aesar), 19.5 mL of squalane and 0.5mL of dibenzyl ether. The brownish mixture was heated at 120 °C under a magnetic stir for 1 hour in order to remove water residues and to homogenize the solution. The magnetic stirrer was then removed and the flask was connected to a reflux condenser before heating the solution to reflux for 1 h with a heating ramp of 5 °C/min. At the end, the mixture was allowed to cool to 120 °C. After cooling at room temperature, the NPs were precipitated by the addition of acetone and washed by agitation with a magnetic stirrer in warm acetone (60°) for 30 minutes. They were then stored in chloroform.
For the second thermal decomposition to synthetize the shell, half of the already washed core NPs stored in chloroform were taken and the chloroform was evaporated with a rotavapor. 0.456 g (0.73 mmol) of cobalt (II) stearate, 0.914 g (1.47mmol) of iron (II) stearate, 1.27 g of oleic acid, 10 mL of dioctyl ether, and 20 mL of 1-octadecene were added to the reaction medium. The mixture was heated to 100 °C for 30 min under magnetic stirring to remove water residues and to homogenize the solution. After removal of the magnetic stirrer, the flask was then connected to a reflux condenser to heat the solution at reflux for another 2 h with a heating ramp of 1 °C/min. After cooling to room temperature, the nanoparticles were precipitated by the addition of acetone to wash them by agitation with a magnetic stirrer in warm acetone (60°) for 1 hour. They were then stored in chloroform.

- CS-4:

A two-necked round-bottom flask was filled with 2 g (2.2 mmol) of commercial iron (III) stearate, 1.24 g of oleic acid (99% Alfa Aesar), and 20 mL of ether dioctyl (BP = 290 °C, 97% Fluka). The brownish mixture was heated at 120 °C under a magnetic stir for 1 hour in order to remove water residues and homogenize the solution. The magnetic stirrer was then removed and the flask was connected to a reflux condenser before heating the solution to reflux for 2 h with a heating ramp of 5 °C/min. At the end, the mixture was allowed to cool to 120 °C. 4 mL of the solution was taken for characterization and after cooling at room temperature, these NPs were precipitated by the addition of acetone and washed by agitation with a magnetic stirrer in warm acetone (60°) for 30 minutes. They were then stored in chloroform.
For the second thermal decomposition to synthesize the shell, 1.16 g (1.84 mmol) of cobalt (II) stearate, 2.36 g (3.68 mmol) of iron (II) stearate, 1.27 g of oleic acid, and 40 mL of 1-octadecene were added to the reaction medium. The mixture was heated to 100 °C for 30 min under magnetic stirring to remove water residues and to homogenize the solution. After removal of the magnetic stirrer, the flask was then connected to a reflux condenser to heat the solution at reflux for another 2 h with a heating ramp of 1 °C/min. After cooling to room temperature, the nanoparticles were precipitated by the addition of acetone to wash them by agitation with a magnetic stirrer in warm acetone (60°) for 1 hour. They were then stored in chloroform.

- $Co_{(1-x)}Fe_{(2+x)}O_4$:

The cobalt ferrite nanoparticles where synthesized using the previously synthesized stearates of iron and cobalt following the already published protocols.[5,6] A two-necked round-bottom flask was filled with 1.24 g (2.0 mmol) of iron (II) stearate, 0.63 g of cobalt (II) stearate, 1.254 g (4.44 mmol) of oleic acid (99% Alfa Aesar) and 20 mL of 1-octadecene (BP = 315 °C, 95% Sigma Aldrich). The brownish mixture was heated at 100 °C under a magnetic stir for 30 min in order to remove water residues and to homogenize the solution. The magnetic stirrer was then removed and the flask was connected to a reflux condenser before heating the solution to reflux for 2 h with a heating ramp of 1 °C/min. At the end, the mixture was allowed to cool to 100 °C. After cooling at room temperature, the NPs were precipitated by the addition of acetone and washed by agitation with a magnetic stirrer in warm acetone (60°) for 30 minutes. They were then stored in chloroform.

2) Transmission electron microscopy (TEM) images of the nanoparticles:

The TEM images were obtained on a JEOL 2100 LaB6 instrument with a 0.2 nm point-to-point resolution. The Fast Fourier Transformation and the microscopy images treatment and analysis were done using the DigitalMicrograph software.
STEM images and EELS data were obtained using a probe-corrected Titan low-base (Thermo Fisher Scientific) equipped with a high-brightness field-emission gun (X-FEG). Convergence angle was 25 mrad and collection angle for HAADF imaging was 48 (60) mrad at

300 (80) keV. HRSTEM images were acquired at 300 keV while EELS data was acquired at 80 keV, except for data on sample CS-4 (Figure 6 in SI). A Gatan Image Filter (GIF) Tridiem ESR 865 spectrometer was employed for EELS data acquisition using an energy dispersion of 0.2 eV/pixel and a collection angle of 68 mrad. Spectral range was chosen to encompass O-K edge (532 eV), Fe-L_3, L_2 edge (708 eV) and Co-L_3,L_2 edge (780 eV). Spatially-resolved EELS maps were acquired using DigiScan (Digital Micrograph) with pixel sizes below 5 Angstrom. EELS data was analyzed with a custom Matlab software. Spectrum-images were denoised using principal component analysis (PCA) and quantified by integrating a 30-eV wide window of the background-subtracted spectra and normalizing with calculated scattering cross sections.
Samples for HRSTEM and EELS measurements were prepared by drop-casting of 2 µL on holey-carbon TEM grids from the chloroform-stabilized NP suspensions diluted 1:50 in ethyl alcohol. After drying, the grids with NPs were washed in a bath of activated C and ethyl alcohol similar to the process described by Li *et al*.[7] to minimize contamination.

3) Dynamic light scattering (DLS):

Measurements were performed using a nanosizer Malvern (nano ZS) zetasizer at a scattering angle of 173°. A measure corresponds to the average of 3 runs of 1min.

4) X-ray diffraction (XRD):

For CS-1 XRD was performed using a Bruker D8 Advance equipped with a monochromatic copper radiation (Kα = 0.154056 nm) and a Sol-X detector in the 20−80° 2θ range with a scan step of 0.02°. High-purity silicon powder (a = 0.543082 nm) was systematically used as an internal standard.
For CS-3 and CS-2, a Bruker D8 Advance equipped with a non-monochromatic copper radiation (Kα = 0.154056 nm) and a Sol-X detector in the 20−80° 2θ range with a scan step of 0.02°. High-purity silicon powder (a = 0.543082 nm) was systematically used as an internal standard.
For CS-4 The XRD measurements were carried out on a D8 Discover diffractometer in Bragg Brentano geometry equipped with a Cu Sealed tube ($\lambda K_{\alpha 1}$ = 1.54059 Å), a quartz front monochromator, a motorized anti-scatter screen and an energy resolved Lynxeye XE-T linear detector. Measurements were performed in the 20−80° 2θ range with a scan step of 0.02°. High-purity silicon powder (a = 0.543082 nm) was systematically used as an internal standard.
For $Co_{(1-x)}Fe_{(2+x)}O_4$ nanoparticles XRD were done on Bruker D8 Advance equipped with a monochromatic copper radiation (Kα = 0.154056 nm) and a Sol-X detector in the 20−80° 2θ range with a scan step of 0.02°. High-purity silicon powder (a = 0.543082 nm) was systematically used as an internal standard.

From the diffractograms, it is possible to extract the cell parameter. This parameter was obtained by fitting the data with fullprof software.

5) Cyclic voltammetry measurements:

The NPs were drop casted on a clean polished glassy carbon electrode (d=0.5 cm) and then a 3-electrode cell was used with a 0.1M NaOH electrolyte to characterize the material electrochemically. The working electrode (WE) is the glassy carbon with the NPs, the counter electrode (CE) is a gold wire, and the reference electrode (RE) is a Hg/HgO electrode which potential vs RHE has been regularly calibrated to make sure that its potential wasn't changing with time.
The first 50 cycles were done between 0.83 and 1.43V *vs.* RHE with a scan rate of 100mV/s in order to clean the surface and to get rid of the oleic acid/ organic molecules that can surround the NPs. Then cycles between 0.83 and 1.73V *vs.* RHE were performed with a 10mV/s scan rate. On these curves that will be corrected from the ohmic losses, the Tafel slope and the activity were determined.
Measurements were performed on a Gamry potentiostat REF 600.
The NPs are in suspension in chloroform, 10 mL were dropcasted directly on the electrode and the chloroform was evaporated, resulting in loading of CS-1, CS-2, CS-3, CS-4 and cobalt ferrite nanoparticles of 0.63, 4.23, 1.43, 2.30 and 1.34 µg cm^{-2}, respectively.

The surface of the NPs used to calculate the activity has been estimated from the average diameter of the NPs assuming spherical shape and that all the surface of the catalyst was involved in the reaction.

6) Impedance measurements:

Impedance measurements were performed with the same sample as for the cyclic voltammetry measurements on the same Gamry REF 600 potentiostat after the cyclic voltammetry measurements at 2 different potentials: 1.63 and 1.68V *vs.* RHE. The range of frequency was from 0.2Hz to 100 kHz with 10 points per decade. These impedance measurements will be used to measure the electrolyte resistance and to correct the ohmic losses in the cyclic voltammetry curves.

7) Depth profiling measurements:

Depth profiling measurements were performed on ISSIS beamline of BESSY synchrotron. The kinetic energies that were used for probing different depths inside the NPs are 150, 200, 300, 400 and 500 eV. The average mean free paths for these energies were

given by QUASES software. The area of the Co2p and Fe2p peaks have been integrated thanks to casa XPS software and the proportion of iron vs cobalt has been calculated using the following formula:

$$C_A = \frac{\frac{I_A}{S_A}}{\sum(\frac{I_n}{S_n})}$$

Where C_A is the atomic concentration of a given element among a number of n elements. I_A---I_n is the area of the peak characteristic of a given element, S_A- - - S_n are the sensitivity factor that depends on the cross-section of the element and also on the flux of the incident source. The cross-sections were taken from ELETTRA synchrotron website[8] and the flux was taken from BESSY flux curve.

Complementary data analysis

1) TEM analysis of the core-shell NPs:

Pristine NPs display a narrow size distribution and spherical shape (**Figure *S*1**).

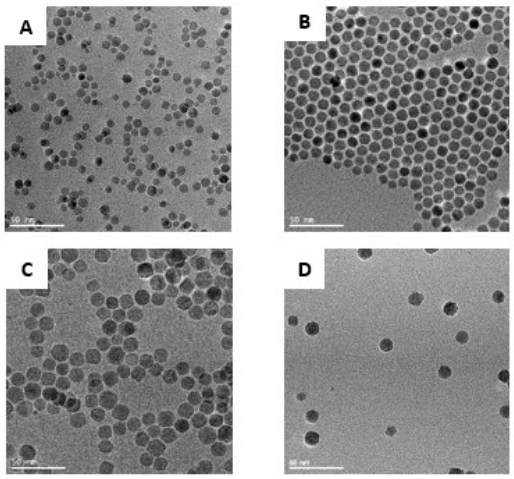

Figure S1: TEM micrographs of pristine Fe_3O_4 NPs used for the synthesis of CS-1 (A), CS-2 (B), CS-3 (C) and CS-4 (D)

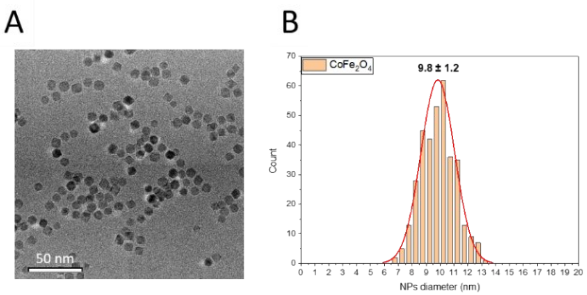

Figure S2: TEM micrograph and size-distribution of $Co_{(1-x)}Fe_{(2+x)}O_4$ NPs

From the TEM micrographs, the size of pristine and core-shell NPs were calculated. Assuming the NPs were perfectly spherical and without considering the diffusion phenomena, it was possible to calculate the volume of the core and the volume of the shell by subtracting the core volume to the core-shell volume. From these volumes, their contribution to the total volume of the NPs was calculated thanks to the following calculation (x being the shell or the core):

$$V_x\% = \frac{V_x}{V_{tot}}$$

From these volume contributions, as in the core there is only iron oxide (100 %) and in the shell, there is 66 % of iron oxide, the theoretical atomic percentage of iron in the NPs was calculated as it follows:

$$V_{shell}\% \times 0.66 + V_{core}\% \times 1 = \%_{at}Fe$$

This proportion was compared to the experimental Co:Fe ratio measured thanks to EDX (**Table *S1***).

Table S1: EDX measured cobalt concentration and theoretical concentration for core-shell NPs

Sample	Co:Fe experimental	Co:Fe theoretical
CS-1	16	9
CS-2	15	3
CS-3	19	9
CS-4	12	12

2) Granulometry analysis:

Granulometry is useful to detect the presence of aggregates in the colloidal suspension of the NPs. The NPs are surrounded by oleic acid that is grafted at their surface, this surfactant is the reason for their stability and non-aggregation. The hydrodynamic diameter (NPs and oleic acid system) was measured (**Figure S3**).

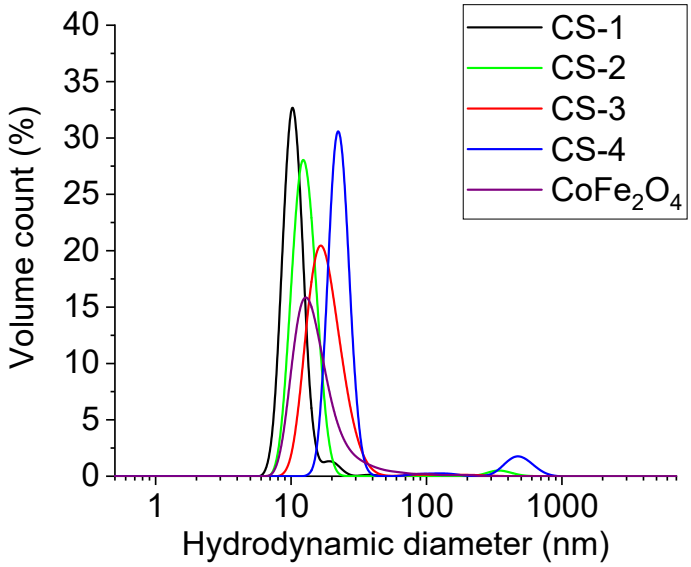

Figure S3: Granulometry measurements. The hydrodynamic diameter is plotted as a function of the volume count for CS-1, CS-2, CS-3, CS-4 and $Co_{(1-x)}Fe_{(2+x)}O_4$

Figure S3 evidences a monomodal distribution of the hydrodynamic diameter in volume counts for all NPs. Some additional contributions can be seen for CS-2 and CS-4 around 300 nm that are characteristic of a few aggregates which can be neglected as they represent a small contribution to the total volume of NPs in the suspension.

3) XRD characterization of the NPs:

The XRD patterns were measured for the core and the core-shell system of all samples (**Figure *S4***).

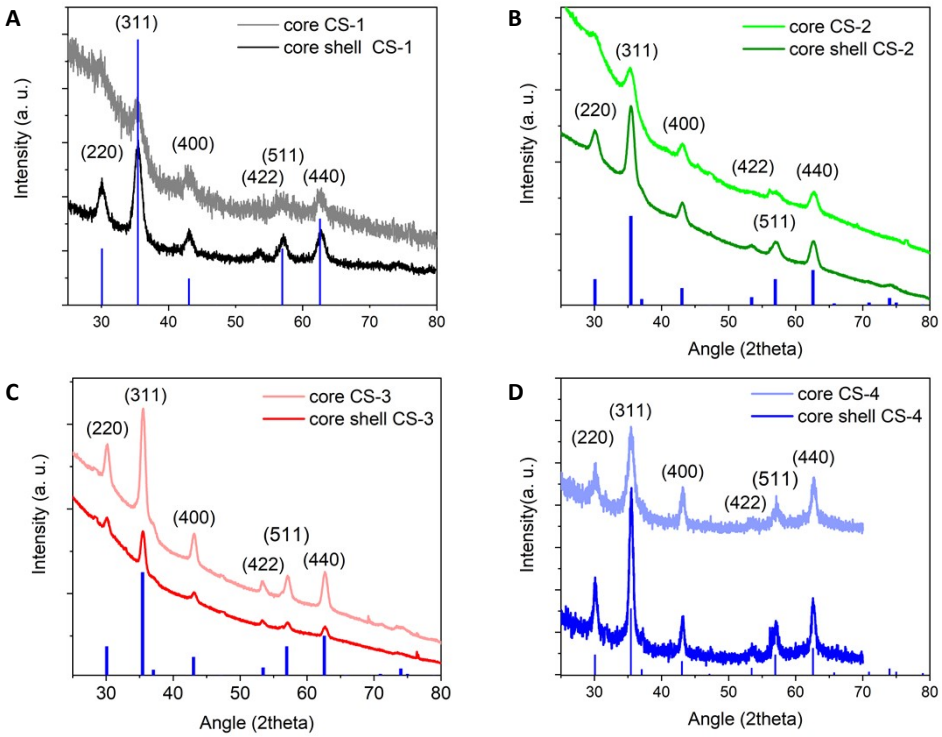

Figure S4: XRD patterns obtained for CS-1 (A), CS-2 (B), CS-3 (C) and CS-4 (D). Bar diagrams correspond to the spinel structure (Fe_3O_4 either $CoFe_2O_4$).

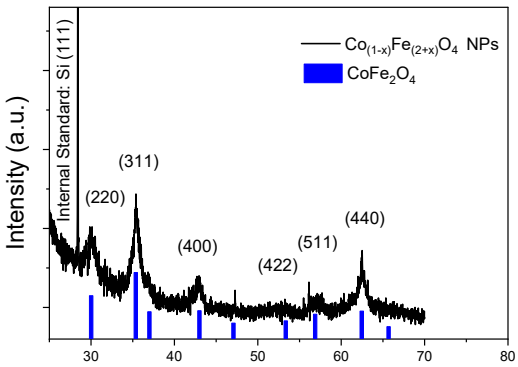

Figure S5: XRD pattern of the synthesized $Co_{(1-x)}Fe_{(2+x)}O_4$ NPs

Figure *S*4 shows that all the NPs present the peaks characteristics of the inverse spinel structure. The $CoFe_2O_4$ and the Fe_3O_4 both having the same structure with almost the same cell parameter (8.396 Å for magnetite and 8.3919 Å for $CoFe_2O_4$), it is not possible to discriminate them on a XRD patterns.
The cell parameters of the different NPs were also calculated using Rietveld refinement thanks to the Fullprof program. The values are given in **Table *S2*** below. It can also be observed that the calculations of the cell parameters for the different NPs are coherent with the values expected in the literature.

Table S2: cell parameters calculated for CS-2, CS-1, CS-3, CS-4

Sample	Cell parameter (Å)
CS-1	Core-shell: 8.3815 ± 0.001
CS-2	Core: 8.395 ± 0.001 Core-shell: 8.386 ± 0.002

CS-3	Core: 8.386 ± 0.001 Core-shell: 8.387 ± 0.004
CS-4	Core: 8.3866 ± 0.003 Core-shell:8.3797 ± 0.006
$Co_{(1-x)}Fe_{(2+x)}O_4$	Shell: 8.3978 ± 0.018

4) EELS and STEM HAADF characterizations of the NPs:

The STEM HAADF images of the NPs are given below (**Figure *S6***). They are crystalline and display lattice fringes distances typical of the spinel structure.

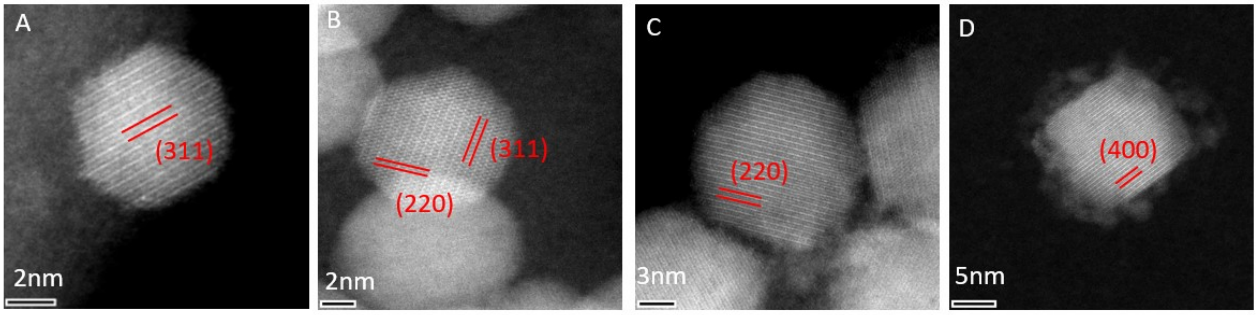

Figure S6: STEM HAADF micrographs of CS-1 (A) and CS-2 (B), CS-3 (C) and CS-4 (D).

The iron and cobalt distribution in the shell can be evidenced thanks to the ratio of the intensities of Fe and Co L-edges in the shell and in the core divided by calculated scattering cross sections. The scattering cross section for Co is slightly higher for Co than for Fe under the used conditions. **Figure *S7*** evidences that the intensity for iron is higher in the core of the NP and that the one of cobalt is higher in the shell which is coherent with a higher density of cobalt in the shell.

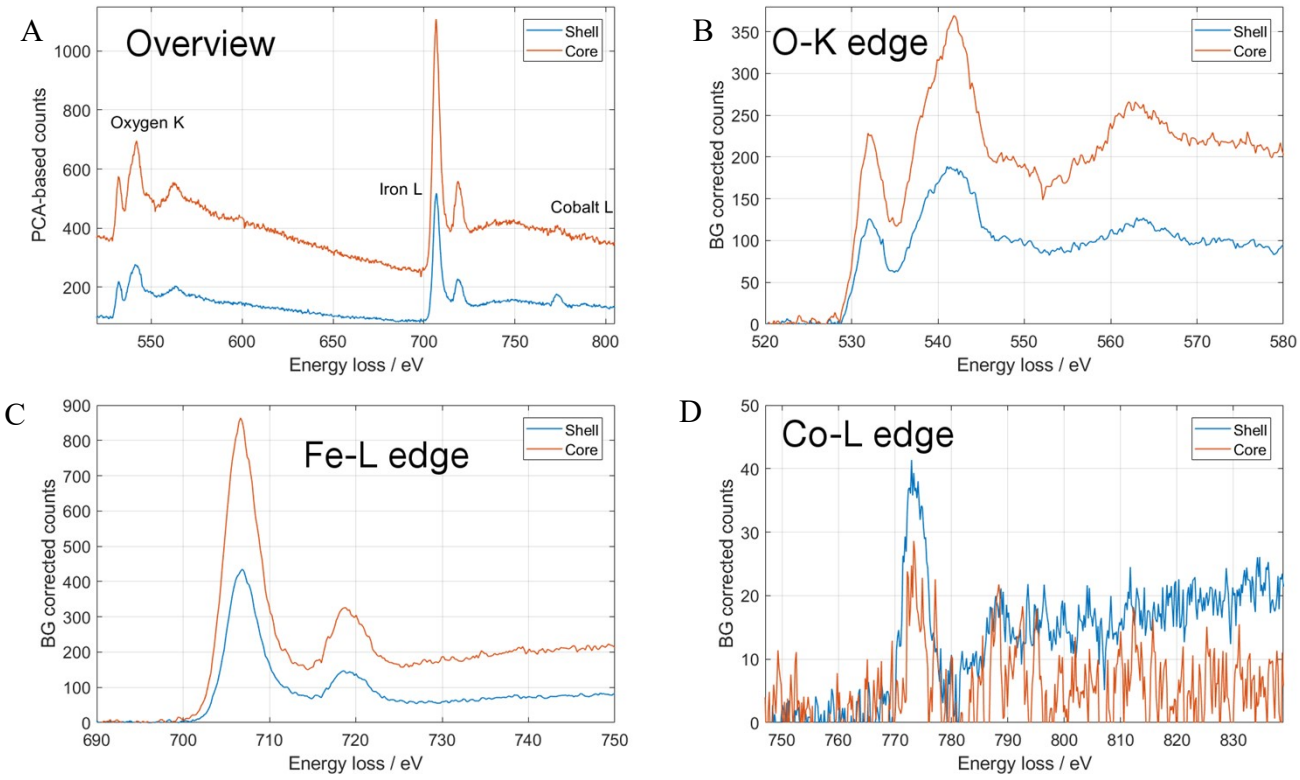

Figure S7: Exemplary EELS spectra obtained from the core and shell region of a NP of the CS-2 sample showing the overview spectrum, the background-corrected spectra of the O-K, the Fe-L, and the Co-L edge.

The thickness of the shell of CS-4 is more important than the one of CS-3 (***Figure S8***). For this sample, the atomic fraction of cobalt is about 14% which is the expected proportion if the material of the shell is $CoFe_2O_4$. This sample presents a larger size distribution than the other synthesis but the shell is sharp and present at the surface of the NPs.

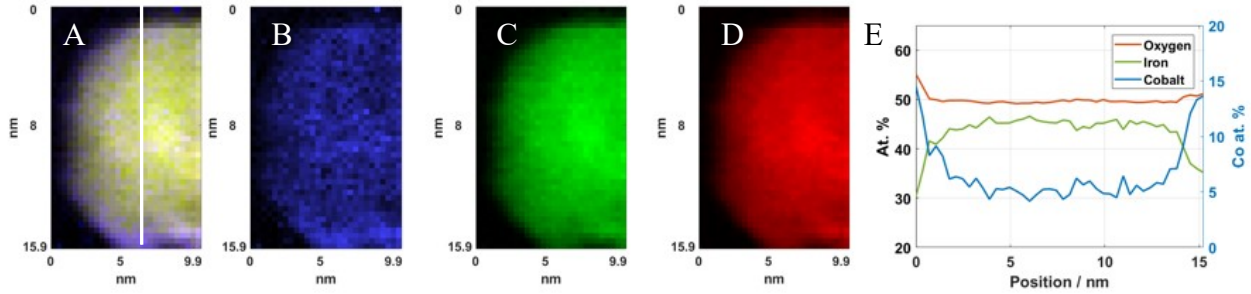

Figure S8: SR-EELS elemental maps : composite (A), cobalt (B), iron (C) and oxygen (D) and profile of element concentration of CS-4 (E) corresponding to the white line in A.

5) Depth profiling measurements

Depth profiling measurements were performed at various incident energies. Indeed, when acquired under the appropriate conditions, one can get a complete quantitative elemental analysis as a function of the depth of the sample: 68 % of all photoelectrons will arise from within a depth of λ (the inelastic mean free path) and 99.7 % will be arising from a 3λ depth[9,10]. The obtained XPS spectra of iron and cobalt have been fitted and the area of the 2p peaks have been calculated (***Figure S9***). This area being proportional to the quantity of the cation, the quantification of the Fe/Co atomic ratio was then possible.

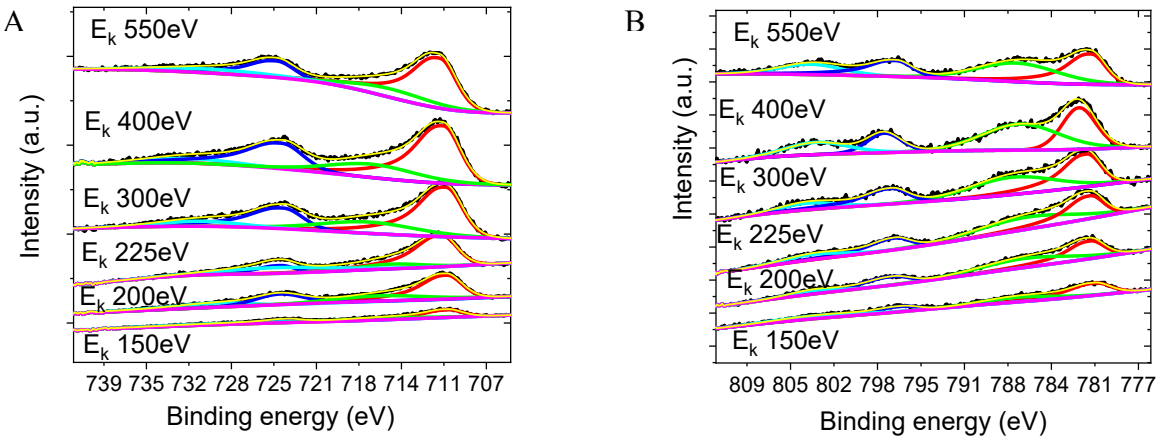

Figure S9: XPS Fe2p peaks (A) and Co2p (rB) spectra and their fitting for different kinetic energies obtained while performing the depth profiling of CS-3. Black: experimental data, yellow: fitting of the experimental data, sum of all the other peaks: 2p3/2 (red) and its satellite (green) as well as 2p1/2 (dark blue) and its satellite (light blue).

6) Tafel slopes

Table S3*:* Tafel slopes for core-shell and $Co_{(1-x)}Fe_{(2+x)}O_4$ NPs extracted from cyclic voltammetry measurements performed in 0.1 M NaOH at 10 mV s^{-1} at two values of the electrode potential 1.62 and 1.67 V vs RHE.

Sample	Tafel slope at 1.62V (mV/decade)	Tafel slope at 1.67V (mV/decade)
CS-1	63 ± 2	76 ± 2
CS-2	52 ± 3	78 ± 3
CS-3	63 ± 2	69 ± 2
CS-4	58 ± 2	72 ± 2

$Co_{(1-x)}Fe_{(2+x)}O_4$	76 ± 5	108 ± 2

6). Selected values of electrocatalytic activities of Co oxides from the literature

The activities of various transition metal oxide catalysts have been reported in the literature. A non-exhaustive list of these activities along with their Tafel slopes and some complementary characteristics (catalyst loading, type and concentration of the electrolyte, as well as carbon addition) are reported in ***Table S4.***

Table S4*:* Mass activities calculated from the literature for different types of catalysts and their Tafel slopes. Data with * have been extrapolated thanks to the values of the Tafel slopes.

Catalyst	Mass activity(A/g)	Tafel slope	Loading (µg/cm²)	Carbon	Electrolyte concentration	reference
$Co(OH)_2$	125*	59	204	Graphene	0.1M KOH	11
CoFe layered double hydroxide	185*	43				
$CoFe_2O_4$ NFs	16	82	429	No carbon	0.1M KOH	12
$CoFe_2O_4$ NPs	2	223				
$CuFe_2O_4$ NFs	0.3	93				
Fe_2O_3 NFs	0.2	148				
$NiFe_2O_4$ NFs	3.4	98				
$CoCr_2O_4$	23.4	177	204	No carbon	0.1M KOH	13
Co_2TiO_4	2.1	83				
$MgCo_2O_4$	120	70				
Co_3O_4	51.6*	61				
Co_3O_4	9.6	83	210	No carbon	0.1M KOH	14
$Co(OH)_2$	12	63				
Fe_3O_4	21	96	960	No carbon	1M KOH	15
Co_3O_4	78	72				
$CoFe_2O_4$	182	58				
Co_3O_4@CoO@Co	56	92	127	No carbon	0.1M KOH	16
Fe_3O_4@CoO	77A/g_{oxide} 154 A/g_{cobalt}*	89	300 (catalyst)	Vulcan XC-72	0.1M KOH	17
Au@Co_3O_4	312A/g_{oxide} 500A/g_{cobalt}*	60	200 (catalyst+carbon) 64 (catalyst) 40 (Co_3O_4)	Vulcan XC-72	0.1M KOH	18
Au@$CoFeO_x$	16 200A/g_{TM}*	58	56 (TM)	Vulcan XC-72	1M KOH	19
Au@$NiCo_2S_4$	50 000A/g_{oxide}*	44.5	200 (catalyst+ carbon)	Carbon black	1M KOH	20
Fe_3O_4	15 A/g_{oxide}	105	100	No carbon	1M KOH	21
$Co_{0.25}Fe_{2.75}O_4$	38 A/g_{oxide} 600 A/g_{cobalt}	80				
$Co_{0.5}Fe_{2.5}O_4$	76 A/g_{oxide} 540 A/g_{cobalt}	45				
$Co_{0.75}Fe_{2.25}O_4$	128 A/g_{oxide} 680 A/g_{cobalt}	46				

$CoFe_2O_4$	128 A/g_{oxide} 510 A/g_{cobalt}	45				
$Co_{1.25}Fe_{1.75}O_4$	165 A/g_{oxide} 528 A/g_{cobalt}	48				
$Co_{1.5}Fe_{1.5}O_4$	232 A/g_{oxide} 620 A/g_{cobalt}	46				
$Co_{1.75}Fe_{1.25}O_4$	261 A/g_{oxide} 600 A/g_{cobalt}	50				
Co_2FeO_4	335 A/g_{oxide} 675 A/g_{cobalt}	50				
$Co_{2.25}Fe_{0.75}O_4$	370 A/g_{oxide} 666 A/g_{cobalt}	52				
$Co_{2.5}Fe_{0.5}O_4$	318 A/g_{oxide} 516 A/g_{cobalt}	47				
$Co_{2.75}Fe_{0.25}O_4$	220 A/g_{oxide} 327 A/g_{cobalt}	56				
Co_3O_4	150 A/g_{oxide}	61				
Co_3O_4	123* A/g_{oxide}	61.8	300	No carbon		
Co_3O_4	240* A/g_{oxide}	80	15	Sibunit	1M NaOH	[22]
Co_3O_4	152* A/g_{oxide}	65	15	BDD		
$CoO_x(OH)_y$ 9nm	5000* A/g_{oxide}	37	2.98			
$CoO_x(OH)_y$ 6nm	5000* A/g_{oxide}	39	0.82			
$CoO_x(OH)_y$ 4nm	11 000* A/g_{oxide}	43	0.82	No carbon	0.1M KOH	[23]
$CoO_x(OH)_y$ 1nm	14 000* A/g_{oxide}	43	0.25			

References

(1) Baaziz, W.; Pichon, B. P.; Fleutot, S.; Liu, Y.; Lefevre, C.; Greneche, J.-M.; Toumi, M.; Mhiri, T.; Begin-Colin, S. Magnetic Iron Oxide Nanoparticles: Reproducible Tuning of the Size and Nanosized-Dependent Composition, Defects, and Spin Canting. *J. Phys. Chem. C* **2014**, *118* (7), 3795–3810. https://doi.org/10.1021/jp411481p.

(2) Sartori, K.; Musat, A.; Choueikani, F.; Grenèche, J.-M.; Hettler, S.; Bencok, P.; Begin-Colin, S.; Steadman, P.; Arenal, R.; Pichon, B. P. A Detailed Investigation of the Onion Structure of Exchanged Coupled Magnetic Fe3−δO4@CoFe2O4@Fe3−δO4 Nanoparticles. *ACS Appl. Mater. Interfaces* **2021**, *13* (14), 16784–16800. https://doi.org/10.1021/acsami.0c18310.

(3) Liu, X.; Pichon, B. P.; Ulhaq, C.; Lefèvre, C.; Grenèche, J.-M.; Bégin, D.; Bégin-Colin, S. Systematic Study of Exchange Coupling in Core–Shell Fe3−δO4@CoO Nanoparticles. *Chem. Mater.* **2015**, *27* (11), 4073–4081. https://doi.org/10.1021/acs.chemmater.5b01103.

(4) Perton, F. Architecture de Nanoparticules Hybrides Pour Une Imagerie et/Ou Thérapie Multimodales. thesis, Strasbourg, 2019. http://www.theses.fr/2019STRAE043 (accessed 2022-03-03).

(5) Cotin, G.; Kiefer, C.; Perton, F.; Boero, M.; Özdamar, B.; Bouzid, A.; Ori, G.; Massobrio, C.; Begin, D.; Pichon, B.; Mertz, D.; Begin-Colin, S. Evaluating the Critical Roles of Precursor Nature and Water Content When Tailoring Magnetic Nanoparticles for Specific Applications. *ACS Appl. Nano Mater.* **2018**, *1* (8), 4306–4316. https://doi.org/10.1021/acsanm.8b01123.

(6) Sartori, K.; Musat, A.; Choueikani, F.; Grenèche, J.-M.; Hettler, S.; Bencok, P.; Begin-Colin, S.; Steadman, P.; Arenal, R.; Pichon, B. P. A Detailed Investigation of the Onion Structure of Exchanged Coupled Magnetic Fe3−δO4@CoFe2O4@Fe3−δO4 Nanoparticles. *ACS Appl. Mater. Interfaces* **2021**, *13* (14), 16784–16800. https://doi.org/10.1021/acsami.0c18310.

(7) Li, C.; Tardajos, A. P.; Wang, D.; Choukroun, D.; Van Daele, K.; Breugelmans, T.; Bals, S. A Simple Method to Clean Ligand Contamination on TEM Grids. *Ultramicroscopy* **2021**, *221*, 113195. https://doi.org/10.1016/j.ultramic.2020.113195.

(8) *WebCrossSections*. https://vuo.elettra.eu/services/elements/WebElements.html (accessed 2022-06-01).

(9) Carlson, T. A.; McGuire, G. E. Study of the X-Ray Photoelectron Spectrum of Tungsten—Tungsten Oxide as a Function of Thickness of the Surface Oxide Layer. *J. Electron Spectrosc. Relat. Phenom.* **1972**, *1* (2), 161–168. https://doi.org/10.1016/0368-2048(72)80029-X.

(10) Strohmeier, B. R. An ESCA Method for Determining the Oxide Thickness on Aluminum Alloys. *Surf. Interface Anal.* **1990**, *15* (1), 51–56. https://doi.org/10.1002/sia.740150109.

(11) Han, X.; Yu, C.; Yang, J.; Zhao, C.; Huang, H.; Liu, Z.; Ajayan, P. M.; Qiu, J. Mass and Charge Transfer Coenhanced Oxygen Evolution Behaviors in CoFe-Layered Double Hydroxide Assembled on Graphene. *Adv. Mater. Interfaces* **2016**, *3* (7), 1500782. https://doi.org/10.1002/admi.201500782.

(12) Li, M.; Xiong, Y.; Liu, X.; Bo, X.; Zhang, Y.; Han, C.; Guo, L. Facile Synthesis of Electrospun MFe2O4 (M = Co, Ni, Cu, Mn) Spinel Nanofibers with Excellent Electrocatalytic Properties for Oxygen Evolution and Hydrogen Peroxide Reduction. *Nanoscale* **2015**, *7* (19), 8920–8930. https://doi.org/10.1039/C4NR07243J.

(13) Liu, Z.; Wang, G.; Zhu, X.; Wang, Y.; Zou, Y.; Zang, S.; Wang, S. Optimal Geometrical Configuration of Cobalt Cations in Spinel Oxides to Promote Oxygen Evolution Reaction. *Angew. Chem. Int. Ed.* **2020**, *59* (12), 4736–4742. https://doi.org/10.1002/anie.201914245.
(14) Masa, J.; Weide, P.; Peeters, D.; Sinev, I.; Xia, W.; Sun, Z.; Somsen, C.; Muhler, M.; Schuhmann, W. Amorphous Cobalt Boride (Co2B) as a Highly Efficient Nonprecious Catalyst for Electrochemical Water Splitting: Oxygen and Hydrogen Evolution. *Adv. Energy Mater.* **2016**, *6* (6), 1502313. https://doi.org/10.1002/aenm.201502313.
(15) Guo, D.; Kang, H.; Wei, P.; Yang, Y.; Hao, Z.; Zhang, Q.; Liu, L. A High-Performance Bimetallic Cobalt Iron Oxide Catalyst for the Oxygen Evolution Reaction. *CrystEngComm* **2020**, *22* (25), 4317–4323. https://doi.org/10.1039/D0CE00401D.
(16) Chou, S.-C.; Tso, K.-C.; Hsieh, Y.-C.; Sun, B.-Y.; Lee, J.-F.; Wu, P.-W. Facile Synthesis of Co3O4@CoO@Co Gradient Core@Shell Nanoparticles and Their Applications for Oxygen Evolution and Reduction in Alkaline Electrolytes. *Materials* **2020**, *13* (12). https://doi.org/10.3390/ma13122703.
(17) Zhou, L.; Deng, B.; Jiang, Z.; Jiang, Z.-J. Shell Thickness Controlled Core–Shell Fe3O4@CoO Nanocrystals as Efficient Bifunctional Catalysts for the Oxygen Reduction and Evolution Reactions. *Chem. Commun.* **2019**, *55* (4), 525–528. https://doi.org/10.1039/C8CC09140D.
(18) Zhuang, Z.; Sheng, W.; Yan, Y. Synthesis of Monodispere Au@Co3O4 Core-Shell Nanocrystals and Their Enhanced Catalytic Activity for Oxygen Evolution Reaction. *Adv. Mater.* **2014**, *26* (23), 3950–3955. https://doi.org/10.1002/adma.201400336.
(19) Strickler, A. L.; Escudero-Escribano, M.; Jaramillo, T. F. Core–Shell Au@Metal-Oxide Nanoparticle Electrocatalysts for Enhanced Oxygen Evolution. *Nano Lett.* **2017**, *17* (10), 6040–6046. https://doi.org/10.1021/acs.nanolett.7b02357.
(20) Lv, Y.; Duan, S.; Zhu, Y.; Yin, P.; Wang, R. Enhanced OER Performances of Au@NiCo2S4 Core-Shell Heterostructure. *Nanomaterials* **2020**, *10* (4), 611. https://doi.org/10.3390/nano10040611.
(21) Saddeler, S.; Bendt, G.; Salamon, S.; Haase, F. T.; Landers, J.; Timoshenko, J.; Rettenmaier, C.; Jeon, H. S.; Bergmann, A.; Wende, H.; Cuenya, B. R.; Schulz, S. Influence of the Cobalt Content in Cobalt Iron Oxides on the Electrocatalytic OER Activity. *J. Mater. Chem. A* **2021**, *9* (45), 25381–25390. https://doi.org/10.1039/D1TA06568H.
(22) Kéranguéven, G.; Filimonenkov, I. S.; Savinova, E. R. Investigation of the Stability of the Boron-Doped Diamond Support for Co3O4-Based Oxygen Evolution Reaction Catalysts Synthesized through in Situ Autocombustion Method. *J. Electroanal. Chem.* **2022**, 116367. https://doi.org/10.1016/j.jelechem.2022.116367.
(23) Haase, F. T.; Bergmann, A.; Jones, T. E.; Timoshenko, J.; Herzog, A.; Jeon, H. S.; Rettenmaier, C.; Cuenya, B. R. Size Effects and Active State Formation of Cobalt Oxide Nanoparticles during the Oxygen Evolution Reaction. *Nat. Energy* **2022**, 1–9. https://doi.org/10.1038/s41560-022-01083-w.

Author Contributions

LR synthesized the electrocatalysts, performed and analyzed the FTIR, DLS, XRD and electrochemical characterization and wrote the initial draft. IM synthesized the $Co_{(1-x)}Fe_{(2+x)}O_4$ nanoparticles, performed and analyzed the FTIR, DLS, XRD, TEM and electrochemical characterization. RA and SH performed and analyzed the STEM HAADF and EELS measurements. TA, BR, LR and AB performed the XPS depth profiling acquisition, which was analyzed by LR. BP, ES and AB provided the original idea, discussed the results and analyses. All authors contributed to the manuscript corrections and read the manuscript.